Chapter 4

High field MRI of single histological slices using an inductively-coupled self-resonant microcoil: application to *ex vivo* samples of patients with Alzheimer's disease

Adapted from NMR Biomed. 2011 May;24(4):351-7

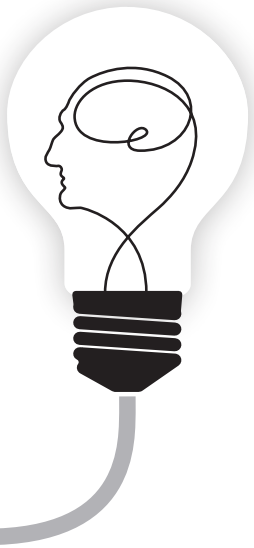

Rob J.A. Nabuurs[1,5]
Ingrid Hegeman[3]
Remco Natté[4]
Sjoerd G. van Duinen[3,4]
Mark A. van Buchem[1]
Louise van der Weerd[1,2,5]
Andrew G. Webb[1]

Abstract

A simple inductively-coupled microcoil has been designed to image tissue samples placed on a microscope slide, samples which can subsequently be stained histologically. As the exact same tissue is used for MRI and histology, the two data sets can be compared without the need for complicated image registration techniques. The design can be integrated into any MRI system using existing commercial hardware. Compared to a commercial 20 mm diameter birdcage, the signal-to-noise was increased by a factor of 3.8, corresponding to a reduction in data acquisition time of ~15. An example is shown of *ex vivo* samples of patients with Alzheimer's disease, in which the co-registration of highly sensitive iron staining and focal plaques is confirmed.

Introduction

MRI is a versatile and powerful tool to study many pathological conditions, both *in vivo* and *ex vivo*. In order to verify that changes in MRI signal intensity are due to pathology, histology remains the gold standard for determining the nature of tissue changes. It is highly challenging to co-register precisely the data from histological sections and MRI, primarily due to the deformations and shrinkage that occur when tissue is processed for histology following MR data acquisition. In addition, histological sections would ideally be cut in exactly the same orientation as the acquired MRI data, but this is in practice not feasible. To overcome these difficulties one can develop image processing algorithms to co-register the histological and MRI data by either attempting to correct for 3D deformations or the difference in spatial orientation.[1] However, even under the most optimal experimental conditions, the very different spatial resolution of MRI and histological sections makes direct registration a cumbersome task.

To alleviate most of these difficulties and possible errors, a straightforward solution is to obtain MR images directly from the same histological slice that is used for staining. Meadowcroft *et al*.[2] have designed and built a highly specialized coil setup for horizontal-bore 3T and 7T scanners, which enables direct MRI of histological sections, such as those used for standard pathology. The imaged tissue slices were afterwards subject to several histological stains, thereby showing it is a worthy addition to study and validate MR contrast changes with respect to its pathological substrate, *e.g.* within Alzheimer's disease (AD) brain tissue. The Meadowcroft coil has excellent sensitivity and performance, but requires relatively specialized expertise to construct and test, and is difficult to implement within the very restricted diameter bore of high field vertical MR magnets. A simple alternative approach would be to use a small self-resonant microcoil placed around the sample, and to inductively couple this coil to the much larger volume resonator which is standardly provided with the system. The principles of inductively coupling a larger transmit coil to a smaller self-resonant "microcoil" have been covered in many publications, with recent comprehensive signal-to-noise ratio (SNR) analyses in articles by Bilgen[3] and Utz[4]. These analyses show that the loss in sensitivity using an inductively coupled arrangement compared to using a microcoil alone is, at most, a few percent. The approach of using inductively coupled self-resonant coils for MR microscopy was first shown by Banson[5], with the approach having been extended by Glover *et al*.[6] to show co-registered optical and MR images of epidermal cells of Alium Cepa.

In the following study, we have designed and characterized an inductively coupled "histological coil" for a 9.4 T vertical magnet. The coil is placed at the back of a standard microscope slide so it completely covers a 60 µm thick tissue sample. Using these easily-produced and replaceable coils, high resolution images of histological samples can be acquired with a ~15 fold reduction in data acquisition time compared to using a commercial resonator. After MRI, the same sample underwent staining. In this case, the samples are from *ex vivo* human brain tissue from an ongoing AD study. After MRI scanning, a double staining was performed by using a new modified Perls' 3,3'-diaminobenzidine (DAB) staining combined with immunofluorescence for amyloid β (Aβ).

Materials and Methods

RF coil design

The RF coil was constructed from pure silver 18 AWG wire, shaped into a square with dimensions 15 x 15 mm, ~20% larger than the histological slices so that areas of inhomogeneous B_1 field very close to the wires do not cover the sample. (**Figure 4.1A**) For maximum SNR the microcoil should be strongly coupled to the outer birdcage coil. If the microcoil is tuned to 400 MHz, this introduces a frequency shift that could not be compensated for by re-adjusting the impedance matching capacitors of the birdcage. Therefore, the microcoil should be self-resonant at a frequency slightly different from 400 MHz. As outlined by Bilgen[3], one can minimize the current in the larger coil by resonating the microcoil at a slightly lower frequency than the larger coil,

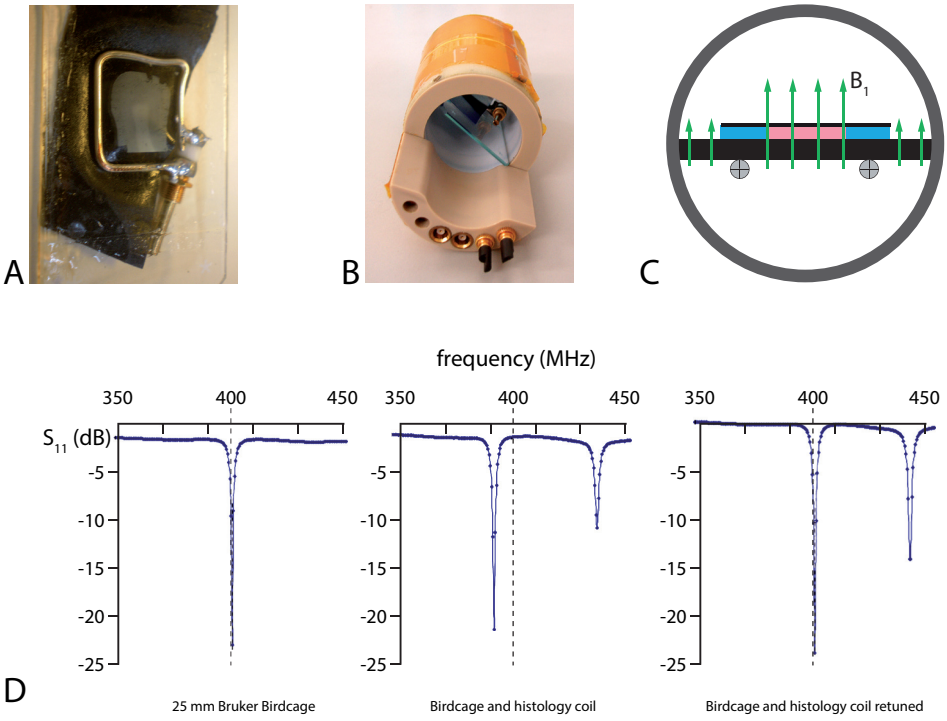

Figure 4.1 Design of the inductively coupled microcoil
The self-resonant coil is taped onto the back of a standard 25 mm wide microscope slide such that it covers a 60 µm thick brain section, which is mounted on the opposite side in PBS 1X (**A**). The slide is positioned in a 25 mm diameter commercial volume resonator (**B**) such it achieves the strongest coupling. Impedance matching of the histology coil is performed by using the variable capacitors of the birdcage coil (black screws). A schematic cross section of the setup is shown in (**C**) with the coil on one side of the microscope slide and the sample on the other. The arrows illustrate how the B1 field is localized due to presence of the inductively coupled coil while applying an RF pulse via the volume resonator. (**D**) Network analyzer S_{11} plots from, respectively, the commercial resonator alone (left), with the strongly coupled coil (center), and after retuning and impedance matched to 50 Ω at 400 MHz.

and then using the lower of the two split-resonances. A 1-3.5 pF non-magnetic variable capacitor (Johansson, Boonton, NY), with a DC breakdown voltage of 1 kV, was used to tune the microcoil to the resonant frequency of ~396 MHz. The coil was placed directly onto the back of a microscopic slide on which the sample had already been placed. (**Figure 4.1A**) Next, the slide was placed in a 25 mm standard Bruker high-pass birdcage resonator (**Figure 4.1B-C**), which was connected to a network analyzer (Agilent Technologies, Santa Clara, CA). The orientation of the slide was adjusted to produce the strongest coupling. The mutual inductance splits the resonance frequency into two separate peaks. The low frequency resonance was impedance matched to 50 Ohms at 400 MHz by adjusting the variable capacitors of the birdcage coil. (**Figure 4.1B-D**)

Sample preparation

Tissue was obtained from The Netherlands Brain Bank (NBB), Netherlands Institute for Neuroscience, Amsterdam. All material has been collected from donors for or from whom a written informed consent for brain autopsy and the use of the material and clinical information for research purposes had been obtained by the NBB. A 12 x 12 x 10 mm formalin-fixed human brain tissue sample was resected from the neocortex and cut into 60 µm-thick sections with a vibratome (VT1000, Leica) followed by immersion in 1X phosphate buffered saline (PBS) for at least 24 hrs to wash out any residual formalin. The tissue section was mounted on a histology slide and a drop of PBS (which had previously been placed under vacuum to reduce air bubbles) was applied to the sample to prevent dehydration. Extreme care was taken to avoid inclusion of any air bubbles by slowly lowering the coverslip, and the section was sealed with nail polish.

MRI data acquisition

All MRI measurements were conducted on a vertical bore 9.4 T Bruker Avance 400 WB spectrometer, with a 1 Tm^{-1} actively shielded gradient insert, equipped with ParaVision 5.0 software running with Topspin 2.0. Pulse width calibrations were performed with a 1 ms hermite pulse. The B_1-field homogeneity of the histology coil was evaluated using the double angle method (DAM) as described by Stollberger and Wach[7] in which two spin echo images were acquired with flip angles = 30º and 60º, TR = 4000 ms, TE = 6.5 ms, 4 signal averages, field of view (FOV) = 16 x 16 mm, and matrix size 64 x 64 complex data points.

Imaging experiments were performed using both gradient- and spin-echo sequences. For all sequences, a slice selection pulse was applied to excite a thickness of 2 mm. Scout gradient echo images were acquired in 1.36 minutes with a FOV of 50 x 50 mm, flip angle = 25°, TR / TE = 75 / 3 ms, matrix = [128 128] and 10 signal averages. Multiple gradient echo images were acquired with flip angle = 22.5°, TR / TE = 75 / 5 -12-19 ms, FOV = 16 x 16 mm, matrix = [256 256] and 200 signal averages resulting in a one hour scan with in-plane resolution of 62 x 62 µm. Multiple spin-echo images were obtained in order to calculate T_2-maps, with TR / TE = 2500 / 10-20-30-40 ms, FOV = 16 x 16 mm, matrix = [128 128] and four averages, obtained in 21 minutes with 125 x 125 μm^2 resolution.

Studies of brain tissue of patients with AD

Several previous studies have shown that the pathological hallmarks of AD, namely Aβ plaques and associated iron deposition, can be detected by MR microscopy.[8,9] In this current study, brain samples from the entorhinal cortex of a confirmed AD patient were prepared. Multiple gradient echo images were acquired with flip angle = 22.5°, TR / TE = 75 / 15 – 25 – 35 - 45 ms, FOV = 16 x 16 mm, matrix = [400 400] and 200 averages resulting in a 1 hour 40 minutes scan with in-plane resolution of 40 x 40 μm^2.

Histological staining

Following MR, the same 60 µm section was double stained using a new modified highly specific Perls' DAB to stain for iron followed by an immunofluorescence Aβ staining. First the free floating section was immersed for 30 min in 100 ml of methanol with 1 ml 30% H_2O_2 and rinsed with subsequently 96% and 70% EtOH in PBS 1X to block endogenous peroxidase. A pretreatment similar to the one described by Levine *et al.*[10,11] was applied at room temperature via 30 minutes of immersion in 1% $NaBH_4$ in PBS followed by 20 minutes in a mixture of 150 µl Proteinase K (Sigma), 50 µl Triton-X 100 and 50 ml PBS. After each step the section was briefly rinsed in PBS 1X before being placed overnight at room temperature in a solution of 7% potassium-hexacyanoferat(II)-trihydrate and 3% HCl according to Smith *et al.*[12] Following rinsing in aquadest and PBS 1X the section was immersed in 100 ml 0.075% DAB (Sigma) with 50 µl 30% H_2O_2 in PBS 1X for 10 minutes after which the reaction was stopped in aquadest.

Next, the same section was immunostained for Aβ using a standard commercial monoclonal antibody immunostaining (6F/3D, DakoCytomation). One hour immersion in 85% formic acid and 30 minutes in trypsin (Type II-S, Sigma), while rinsing with aquadest and PBS 1X in between, was followed by overnight staining in 1 ml 1:10 dilution of Aβ-antibody at room temperature. Secondary antibody staining consisted of 2 hours immersion with 1:100 goat-antimouse-Alexa594 (Invitrogen) for fluorescence microscopy.

Coregistration and image analysis

Histological images were acquired using a Leica DM/RB microscope equipped with a DFC-420c CCD camera and Leica LAC software. For immunofluorescence, images were acquired in a similar fashion with a XBO xenon lamp and Texas Red filterblock N2.1. All subsequent images were taken with a either a 5 or 10 x objective lens allowing automatic photomerging with Adobe Photoshop CS2 to reconstruct a larger image field. A single image was formed from the MR data by summating all the individual echoes of the MGE sequence. Finally, MR and histology data were coregistered based upon matching section outlines and structural features.

Results

RF coil characterization

The frequency shift when the microcoil was placed in the birdcage coil, oriented for maximum coupling, was approximately 10 MHz, as shown in **Figure 4.1D**, with a very small change in the impedance match. The birdcage coil was retuned to 400 MHz using the standard variable

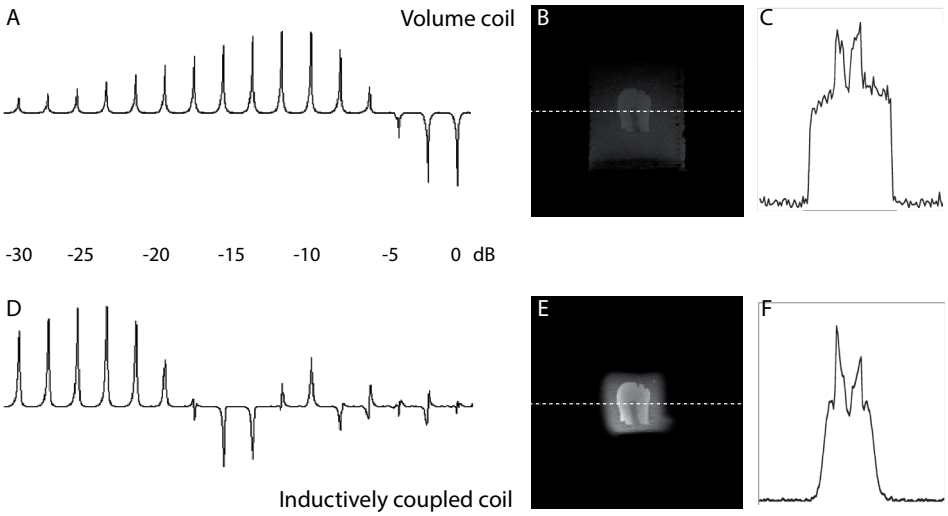

Figure 4.2
Pulse width calibrations (on log scale) for the commercial resonator alone (**A**) and with the coupled histology coil (**B**) showing a 12 dB reduction in power. Identical scout images obtained from a 60 µm brain section with their corresponding profile through the horizontal center of the volume resonator without (**B-C**) and with the histology coil (**E-F**). Besides illustrating the focused B1-field, note the decreased noise in (F) compared to (C).

impedance matching capacitors, and the resulting Q of the retuned coil was almost identical to the birdcage alone. Pulse width calibrations for the 25 mm diameter volume resonator with and without the coupled microcoil showed a decrease of 12 dB in power needed for a 90° pulse when using the inductively coupled coil. (**Figure 4.2A**) The SNR was calculated using the MR images shown in **Figure 4.2B**, with a measured SNR increase of a factor 3.8 when using the coupled system, which corresponds to a reduction in imaging time of a factor of almost 15. The factor of 3.8 is very close to the expected value of 4 based upon the relative 90° pulse widths. The images in **Figure 4.2B** also demonstrate how the B_1-field is localized when using inductively coupled coils, thereby following the concept shown in **Figure 4.1C**. While the PBS surrounding the brain sample is still seen beyond the edges of the coupled coil in the image acquired solely with the volume resonator, this signal is not picked up when using the coupled coil due to localization of the B_1 field.

The experimentally measured B_1-field map shows that excitation is homogenous within the strongly coupled coil. (**Figure 4.3**) The homogeneity measured over a field-of-view of 80% of each of the linear dimensions of the coil showed a standard deviation of ~5% in the B_1-field. Similar to a standard surface coil, this homogeneity quickly drops off at the edges of the coil. The excellent homogeneity produced by the coupled coil makes it possible to obtain accurate quantitative maps of relaxation parameters, such as T_2.

Initial scans to compare the performance of the volume coil versus the coupled system clearly illustrate the gain in SNR when similar scans were obtained. Standard gradient echo images acquired with the coupled coil shows features that are not distinguishable using the volume coil alone. (**Figure 4.4**) Besides clearly distinguishable areas of gray (GM) and white matter (WM),

smaller structures within the GM are also visible. Similar results were obtained when using a standard multiple spin echo sequence at a slightly lower resolution. (**Figure 4.5**) Besides increased SNR and image quality, using the coupled coil allowed the calculation of more accurate T_2 and T_2* maps for obtaining quantitative measurements.

Application to *ex vivo* human AD tissue

Previous literature has strongly suggested that in human AD brain tissue deposits of Aβ, either colocalized with iron or in the absence of any iron, can create hypointense foci upon T_2*-weighted sequences.[2,8,9,13] If the spatial resolution of the MRI is sufficiently high, this allows direct correlation with histology. **Figure 4.6** shows a T_2*-weighted MR image of a tissue section

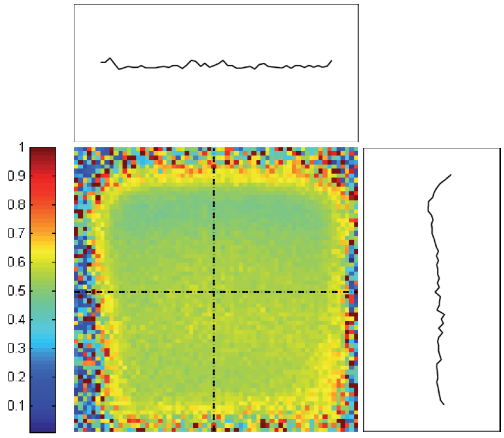

Figure 4.3 B_1-field map
Profiles through the horizontal and vertical center demonstrate the uniformity of the coil within the imaging region of a 60 µm thick brain section.

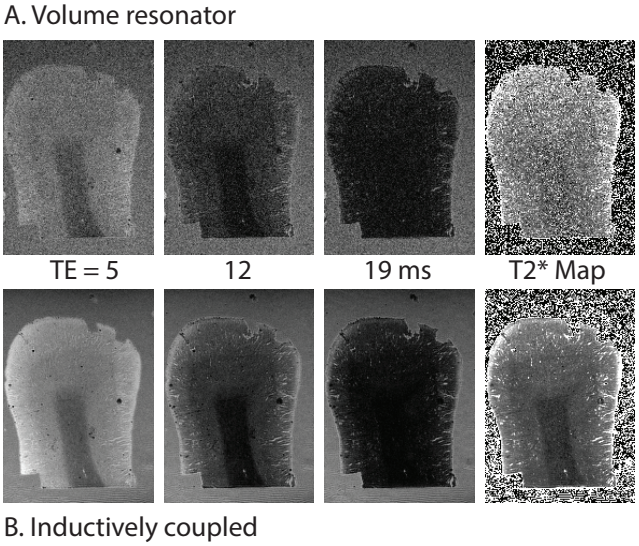

Figure 4.4
Multiple gradient echo images and their corresponding T_2*-map from a 60 µm thick brain section obtained with the volume resonator without (**A**) and with the inductively coupled histology coil (**B**).

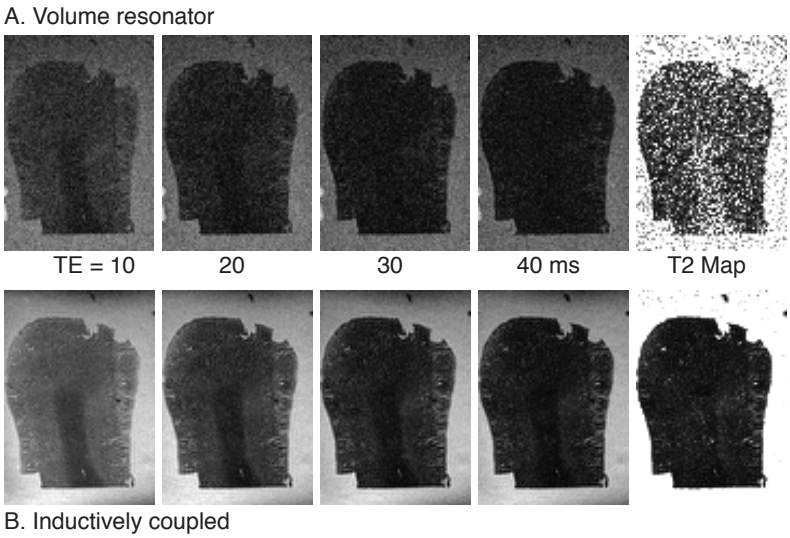

Figure 4.5
Multiple spin echo images and their corresponding T_2-map from a 60 µm thick brain section obtained with the volume resonator without (**A**) and with the inductively coupled histology coil (**B**).

from the entorhinal cortex of an AD patient and its corresponding histological images double stained with a modified Perls' stain for iron and immunofluorescence staining for Aβ. Registration was simply performed based upon the section's outline and structural features: the WM vasculature in particular could easily be correlated in both image modalities due to the high resolution and SNR of the MRI. When examining the complete section, WM and GM are clearly distinguishable in both modalities, in agreement with previous work[2,9] which ascribed the decreased WM signal intensity to an increased iron content of oligodendrocytes and myelin sheets within the WM as confirmed by our modified Perls' staining. Within the MR image, the GM shows many small hypointense foci. A similar distribution of dark brown patches in the iron staining indicated regions of high focal iron content. (**Figure 4.6A-B**) Furthermore, the diffuse brown background coloration within the GM on the iron stain shows a similar distribution to the reduced signal intensity on the MR image.

In order to allow a more detailed evaluation and a direct correlation between the findings on MR and histology, images were zoomed on a selected region outlined by the dashed box. (**Figure 4.6C-E**) As depicted by the yellow arrows, many of the MR hypointense foci indeed represent a one-to-one coregisteration with these dark brown areas of high focal iron content. However, for distinct areas marked by a more diffuse brown colour, suggesting a lower iron concentration, a clear direct correlation could not be made.

When examined carefully, immunostaining for Aβ showed a high Aβ content throughout the GM with almost all deposits correlating with some degree of DAB enhancement of the Perls' staining. (**Figure 4.6E**) On the other hand, while most areas showing an increased iron content were surrounded or covered by Aβ, several small roundish foci did not correlate with Aβ.

According to their location and size these might be iron loaded microglia cells. Not all MR hypo-intensities could be directly correlated with either staining (**Figure 4.6**, *green arrows*), suggesting another source responsible for creating these contrast changes. Since some of these hypo-intensities can also be seen outside the tissue section, this suggests they are likely to be caused by either small impurities or tiny air bubbles.

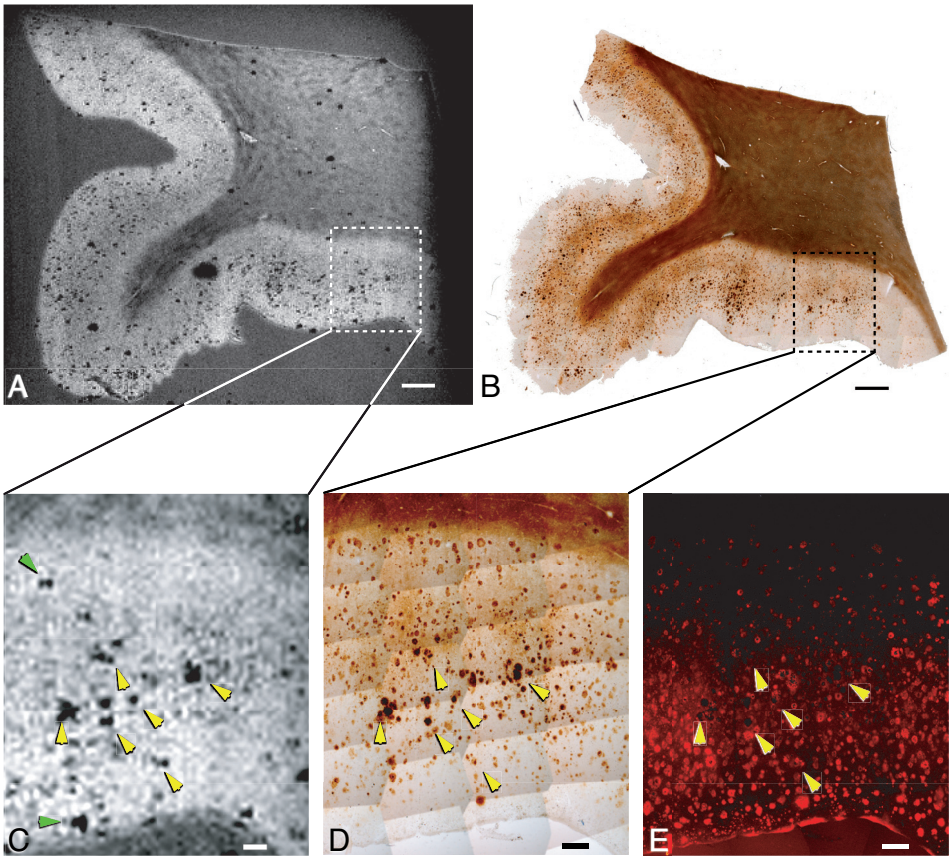

Figure 4.6 MR microscopy of an Alzheimer's disease brain section
(**A**) T_2*-weighted image of a 60 µm brain section of the entorhinal cortex of a known Alzheimer's disease patient. (**B**) Microscopy image of the same section after the new modified Perls' DAB staining for iron. Dark regions indicate higher iron concentration. For more detailed comparison a selected region was enlarged as outlined by the dashed boxes, showing respectively the T_2*-weighted MR image (**C**), iron staining (**D**) and Aβ immunostaining (**E**) of the same section. Many hypointense spots within the MR images clearly coregister with focal iron accumulations (*yellow arrows*), which further colocalizes with Aβ as seen on (**E**). However not all hypo-intensities could be coregistered with either one of the histological stainings (*green arrows*), which might also be caused by image artifacts, like tiny airbubbles. Scale bars represent 1000 µm in (A) and (B), and 200 µm in (C-E).

Discussion

The results presented here indicate that inductively coupled microcoils provide a simple and robust method to acquire high quality MR images of a single histological section in a reasonable data acquisition time. This offers an alternative approach to study various pathological conditions with MR microscopy allowing contrast changes to be easily validated by direct correlation with histology.

Compared to other approaches, these coils are easy to produce, and also to replace if needed. Made to fit around a histological section of any shape, they are broadly applicable to both horizontal and vertical bore systems, and can be impedance-matched up to frequencies well over 1 GHz. Positioned on the back of a microscopic slide, the thickness of the histological section can be varied without the need for additional hardware changes. The high resolution images obtained in this study show sufficiently high SNR such that slices thinner than the current 60 µm should be possible to image, with even better potential correlation with standard histology.

In this study, formalin-fixed samples were cut using a vibratome and immersed in PBS several hours prior to imaging, rather than cryosectioning frozen tissue as was done in previous work.[9] The formalin fixation procedure is known to change MR parameters, but these are partly reversible by PBS immersion. Any extra steps in the slice preparation protocol could lead to additional differences with the *in vivo* situation, and should therefore best be avoided.[9,14,15]

The debate on the exact origin of MRI contrast of amyloid plaques is ongoing, but recent work by Meadowcroft *et al*. shows both dense amyloid accumulations and iron deposits appear to play a role.[9] Within human AD material they showed that focal iron load in amyloid plaques registered well with increased transverse relaxation rates. In contrast, in their mouse model similar effects were seen even in plaques lacking significant iron accumulation, suggesting the interaction of water with the highly compacted amyloid fibril masses as a possible cause for the increased relaxation rates. However, they also showed that the standard Perls' DAB staining is not sensitive enough to the levels of iron present, while a modified protocol was able to show minute amounts of iron even in some of these murine plaques. Applying these modified protocols to 60 µm formalin-fixed human tissue however, high unspecific background staining hampered clear interpretation, as observed by Meadowcroft *et al*.[9] and our own studies (data not shown). As we were unable to exploit the more sensitive iron staining in human material, several questions remain unanswered, e.g. whether diffuse plaques have any effect upon MRI contrast at all, due either to iron or Aβ deposits. Therefore, several adjustments were made to previously published modified Perls' DAB staining protocols focusing on iron accumulation within Aβ deposits of AD brain tissue.[10,12] To lower non-iron-specific DAB enhancement, endogenous peroxidase was blocked using methanol before applying the pretreatment described by LeVine *et al*.[10] The Prussian blue reaction, involving binding of iron(II) containing ferrocyanide to iron(III) within the tissue, was employed using concentrations as described in Smith *et al*.[12] Next, the peroxidase-like H_2O_2-dependent oxidation of DAB used to enhance the iron staining was performed in PBS rather than in aquadest.[16] In our hands, the DAB enhancement was best if applied for 2 minutes. Employing our modified Perls' DAB staining on AD brain tissue resulted in similar iron plaques-like structures, as previously described by LeVine

et al.[10], while the low unspecific background staining allows a more accurate registration with MR then described previously using the modified Perls' staining. Besides these high focal iron depositions many local iron accumulations, which had previously remained undetected, emerged from the background. (**Figure 4.6C**) The more diffuse iron staining, observed in a sublayer of the cortex, could also be detected on the corresponding MR image, in agreement with recent findings by Duyn *et al*. *in vivo*.[17] This global iron distribution should not be mistaken for unspecific background staining; in the latter case, the entire cortex would be stained, and the MRI findings would not correspond.

Although this modified staining technique improves the ability to correlate MR signal changes to focal and diffuse iron concentrations, it has a major disadvantage in that staining for amyloid by standard Thioflavin T or S is not possible, probably due to the very dark pigmentation of the iron-stained sample. Since Thioflavin T or S is an indicator of amyloid (as opposed to Aβ), a correlation between the localization of iron and amyloid is not possible. The immunofluorescence stain does detect the presence of Aβ, but without the ability to discriminate between dense core amyloid and diffuse plaques containing only fibrilar Aβ. Therefore, using our method we obtain much higher iron staining efficiency, but as a consequence we cannot make any statements as to whether the MR hypo-intensities correspond only to iron co-localized with a specific type of Aβ deposition and/or amyloid. Nevertheless, we can conclude that almost all Aβ deposits, whether diffuse plaques or amyloid, contained traces of iron detected by our modified staining, confirming the results of Meadowcroft *et al*. in human *ex vivo* brain. (**Figure 4.6**)

References

1. Breen, MS, Lazebnik, RS, and Wilson, DL. Three-dimensional registration of magnetic resonance image data to histological sections with model-based evaluation. Ann Biomed Eng. 2005; 33:1100-1112.
2. Meadowcroft, MD, Zhang, S, Liu, W, *et al*. Direct magnetic resonance imaging of histological tissue samples at 3.0T. Magn Reson Med. 2007; 57:835-841.
3. Bilgen, M. Inductively-overcoupled coil design for high resolution magnetic resonance imaging. Biomed Eng Online. 2006; 5:3.
4. Utz, M and Monazami, R. Nuclear magnetic resonance in microfluidic environments using inductively coupled radiofrequency resonators. J Magn Reson. 2009; 198:132-136.
5. Banson, ML, Cofer, GP, Black, R, *et al*. A probe for specimen magnetic resonance microscopy. Invest Radiol. 1992; 27:157-164.
6. Glover, PM, Bowtell, RW, Brown, GD, *et al*. A microscope slide probe for high resolution imaging at 11.7 Tesla. Magn Reson Med. 1994; 31:423-428.
7. Stollberger, R and Wach, P. Imaging of the active B_1 field *in vivo*. Magn Reson Med. 1996; 35:246-251.
8. Benveniste, H, Einstein, G, Kim, KR, *et al*. Detection of neuritic plaques in Alzheimer's disease by magnetic resonance microscopy. Proc Natl Acad Sci U S A. 1999; 96:14079-14084.
9. Meadowcroft, MD, Connor, JR, Smith, MB, *et al*. MRI and histological analysis of beta-amyloid plaques in both human Alzheimer's disease and APP/PS1 transgenic mice. J Magn Reson Imaging. 2009; 29:997-1007.
10. LeVine, SM. Iron deposits in multiple sclerosis and Alzheimer's disease brains. Brain Res. 1997; 760:298-303.
11. LeVine, SM. Oligodendrocytes and myelin sheaths in normal, quaking and shiverer brains are enriched in iron. J Neurosci Res. 1991; 29:413-419.
12. Smith, MA, Harris, PL, Sayre, LM, *et al*. Iron accumulation in Alzheimer disease is a source of redox-generated free radicals. Proc Natl Acad Sci U S A. 1997; 94:9866-9868.
13. van Rooden, S, Maat-Schieman, ML, Nabuurs, RJ, *et al*. Cerebral amyloidosis: post-mortem detection with human 7.0-T MR imaging system. Radiology. 2009; 253:788-796.
14. Pfefferbaum, A, Sullivan, EV, Adalsteinsson, E, *et al*. Post-mortem MR imaging of formalin-fixed human brain. Neuroimage. 2004; 21:1585-1595.
15. Shepherd, TM, Thelwall, PE, Stanisz, GJ, *et al*. Aldehyde fixative solutions alter the water relaxation and diffusion properties of nervous tissue. Magn Reson Med. 2009; 62:26-34.
16. Danielisova, V, Gottlieb, M, and Burda, J. Iron deposition after transient forebrain ischemia in rat brain. Neurochem Res. 2002; 27:237-242.
17. Duyn, JH, van, GP, Li, TQ, *et al*. High-field MRI of brain cortical substructure based on signal phase. Proc Natl Acad Sci U S A. 2007; 104:11796-11801.

PART ONE | Native MRI contrast

1 Department of Radiology, Leiden University Medical Center, Leiden, Netherlands
2 Department of Pathology, Leiden University Medical Center, Leiden, Netherlands
3 Department of Neurology, Leiden University Medical Center, Leiden, Netherlands
4 Division of Image Processing (LKEB), Department of Radiology, Leiden University Medical Center, Leiden, Netherlands
5 Department of Pathology, VU University Medical Center, Amsterdam, Netherlands
6 Department of Anatomy & Embryology, Leiden University Medical Center, Leiden, Netherlands
7 Department of Human Genetics, Leiden University Medical Center, Leiden, Netherlands